

Ancilla Assisted Quantum State Tomography in Many-Qubit Registers

Abhishek Shukla¹, K. Rama Koteswara Rao², and T. S. Mahesh^{1*}

¹*Department of Physics and NMR Research Center,*

Indian Institute of Science Education and Research, Pune 411008, India

²*Department of Physics and NMR Research Centre, Indian Institute of Science, Bangalore, India*

The standard method of Quantum State Tomography (QST) relies on the measurement of a set of noncommuting observables, realized in a series of independent experiments. Ancilla Assisted QST (AAQST) proposed by Nieuwenhuizen and co-workers (Phys. Rev. Lett., **92**, 120402 (2004)) greatly reduces the number of independent measurements by exploiting an ancilla register in a known initial state. In suitable conditions AAQST allows mapping out density matrix of an input register in a single experiment. Here we describe methods for explicit construction of AAQST experiments in multi-qubit registers. We also report nuclear magnetic resonance studies on AAQST of (i) a two-qubit input register using a one-qubit ancilla in an isotropic liquid-state system and (ii) a three-qubit input register using a two-qubit ancilla register in a partially oriented system. The experimental results confirm the effectiveness of AAQST in such many-qubit registers.

PACS numbers: 03.67.Lx, 03.67.Ac, 03.65.Wj, 03.65.Ta

Keywords: state tomography, ancilla register, density matrix tomography

I. INTRODUCTION

Quantum computers have the potential to carry-out certain computational tasks with an efficiency that is beyond the reach of their classical counterparts [1]. In practice however, harnessing the computational power of a quantum system has been an enormously challenging task [2]. The difficulties include imperfect control on the quantum dynamics and omnipresent interactions between the quantum system and its environment leading to an irreversible loss of quantum coherence. In order to optimize the control fields and to understand the effects of environmental noise, it is often necessary to completely characterize the quantum state. In experimental quantum information studies, Quantum State Tomography (QST) is an important tool that is routinely used to characterize an instantaneous quantum state [1].

QST on an initial state is usually carried out to confirm the efficiency of initialization process. Though QST of the final state is usually not part of a quantum algorithm, it allows one to measure the fidelity of the output state. QSTs in intermediate stages often help experimentalists to tune-up the control fields better.

QST can be performed by a series of measurements of noncommuting observables which together enables one to reconstruct the complete complex density matrix. In the standard method, the required number of independent experiments grows exponentially with the number of input qubits [3, 4]. Anil Kumar and co-workers have illustrated QST using a single two-dimensional NMR spectrum [5]. They showed that a two-dimensional NMR ex-

periment consisting of a series of identical measurements with systematic increments in evolution time, can be used to quantitatively estimate all the elements of the density matrix. Later Nieuwenhuizen and co-workers have shown that it is possible to reduce the number of independent experiments in the presence of an ancilla register initialized to a known state [6]. They pointed out that in suitable situations, it is possible to carry-out QST with a single measurement of a set of factorized observables. We refer to this method as Ancilla Assisted QST (AAQST). This method was experimentally illustrated by Suter and co-workers using a single input qubit and a single ancilla qubit [7]. Recently Peng and coworkers have studied the effectiveness of the method for qutrit-like systems using numerical simulations [8].

Single shot mapping of density matrix by AAQST method not only reduces the experimental time, but also alleviates the need to prepare the target state several times. Often slow variations in system Hamiltonian may result in systematic errors in repeating the state preparation. Further, environmental noises lead to random errors in multiple preparations. These errors play important roles in the quality of the reconstruction of the target state. Therefore AAQST has the potential to provide a more reliable way of tomography.

In this article we first revisit the theory of QST and AAQST and provide methods for explicit construction of the constraint matrices, which will allow extending the tomography procedure for large registers. An important feature of the method described here is that it requires only global rotations and short evolutions under the collective internal Hamiltonian. We also describe nuclear magnetic resonance (NMR) demonstrations of AAQST on two different types of systems: (i) a two-qubit input

* mahesh.ts@iiserpune.ac.in

register using a one-qubit ancilla in an isotropic liquid-state system and (ii) a three-qubit input register using a two-qubit ancilla register in a partially oriented system.

In the following section we briefly describe the theory of QST and AAQST. In section III we describe experimental demonstrations and finally we conclude in section IV.

II. THEORY

A. Quantum State Tomography

We consider an n -qubit register formed by a system of n mutually interacting spin-1/2 nuclei with distinct resonance frequencies ω_i and mutual interaction frequencies $2\pi J_{ij}$. The Hamiltonian under weak-interaction limit ($2\pi J_{ij} \ll |\omega_i - \omega_j|$) consists of the Zeeman part and spin-spin interaction part, i.e.,

$$\mathcal{H} = -\sum_{i=1}^n \omega_i \sigma_z^i / 2 + \sum_{i=1}^n \sum_{j=i+1}^n 2\pi J_{ij} \sigma_z^i \sigma_z^j / 4 \quad (1)$$

respectively, where σ_z^i and σ_z^j are the z -components of Pauli operators of i th and j th qubits [9]. The set of $N = 2^n$ eigenvectors $\{|m_1 m_2 \dots m_n\rangle\}$ of the Zeeman Hamiltonian form a complete orthonormal computational basis. We can order the eigenvectors based on the decimal value m of the binary string $(m_1 \dots m_n)$, i.e., $m = m_1 2^{n-1} + \dots + m_n 2^0$.

The general density matrix can be decomposed as $\mathbb{1}/N + \epsilon \rho$ where the identity part is known as the background, the trace-less part ρ is known as the *deviation density matrix*, and the dimensionless constant ϵ is the purity factor [10]. In this context, QST refers to complete characterization of the deviation density matrix, which can be expanded in terms of $N^2 - 1$ real unknowns:

$$\begin{aligned} \rho = & \sum_{m=0}^{N-2} \rho_{mm} (|m\rangle\langle m| - |N-1\rangle\langle N-1|) \\ & + \sum_{m=0}^{N-2} \sum_{m'=m+1}^{N-1} \{R_{mm'} (|m\rangle\langle m'| + |m'\rangle\langle m|) \\ & + iS_{mm'} (|m\rangle\langle m'| - |m'\rangle\langle m|)\}. \end{aligned} \quad (2)$$

Here first part consists of $N - 1$ diagonal unknowns ρ_{mm} with the last diagonal element $\rho_{N-1, N-1}$ being constrained by the trace-less condition. R and S each consisting of $(N^2 - N)/2$ unknowns correspond to real and imaginary parts of the off-diagonal elements respectively. Thus a total of $N^2 - 1$ real unknowns needs to be determined.

Usually an experimental technique allows a particular set of observables to be measured directly. To explain the NMR case, we introduce n -bit binary strings, $j_\nu = \nu_1 \nu_2 \dots \nu_{j-1} 0 \nu_j \dots \nu_{n-1}$ and $j'_\nu = \nu_1 \nu_2 \dots \nu_{j-1} 1 \nu_j \dots \nu_{n-1}$ differed only by the flip of the

j th bit. Here $\nu = \nu_1 2^{n-2} + \nu_2 2^{n-3} + \dots + \nu_{n-1} 2^0$ is the value of the $n - 1$ bit binary string $(\nu_1, \nu_2, \dots, \nu_{n-1})$ and ν can take a value between 0 and $\gamma = N/2 - 1$. The real and imaginary parts of an NMR signal recorded in a quadrature mode corresponds to the expectation values of transverse magnetization observables $\sum_{j=1}^n \sigma_{jx}$ and $\sum_{j=1}^n \sigma_{jy}$ respectively [9].

The background part of the density matrix neither evolves under unitaries nor gives raise to any signal, and therefore we ignore it. Under suitable conditions (when all the transitions are resolved), a single spectrum directly yields nN matrix elements $\{R_{j_\nu, j'_\nu}, S_{j_\nu, j'_\nu}\}$ as complex intensities of spectral lines. These matrix elements are often referred to as single quantum elements since they connect eigenvectors related by the flip of a single qubit. We refer the single-quantum terms R_{j_ν, j'_ν} and S_{j_ν, j'_ν} respectively as the real and imaginary parts of ν th spectral line of j th qubit. Thus a single spectrum of an n -qubit system in an arbitrary density matrix can yield nN real unknowns.

In order to quantify the remaining elements, one relies on multiple experiments all starting from the same initial state ρ . The k th experiment consists of applying a unitary U_k to the state ρ , leading to $\rho^{(k)} = U_k \rho U_k^\dagger$, and measuring the single-quantum spectrum $\{R_{j_\nu, j'_\nu}^{(k)}, S_{j_\nu, j'_\nu}^{(k)}\}$. From eqn. (2) we obtain

$$\begin{aligned} R_{j_\nu, j'_\nu}^{(k)} = & \sum_m a_{j_\nu}^{(k)}(m) \rho_{mm} + \\ & \sum_{m, m' > m} c_{j_\nu}^{(k)}(m, m') R_{mm'} + e_{j_\nu}^{(k)}(m, m') S_{mm'}, \\ S_{j_\nu, j'_\nu}^{(k)} = & \sum_m b_{j_\nu}^{(k)}(m) \rho_{mm} + \\ & \sum_{m, m' > m} d_{j_\nu}^{(k)}(m, m') R_{mm'} + f_{j_\nu}^{(k)}(m, m') S_{mm'}, \end{aligned} \quad (3)$$

in terms of the unknowns $\rho_{mm'}$ and the known real constants $\{a, \dots, f\}$:

$$\begin{aligned} a_{j_\nu}^{(k)}(m, m) + i b_{j_\nu}^{(k)}(m, m) = & \langle j_\nu | U_k | m \rangle \langle m | U_k^\dagger | j'_\nu \rangle - \\ & \langle j_\nu | U_k | N-1 \rangle \langle N-1 | U_k^\dagger | j'_\nu \rangle, \\ c_{j_\nu}^{(k)}(m, m') + i d_{j_\nu}^{(k)}(m, m') = & \langle j_\nu | U_k | m \rangle \langle m' | U_k^\dagger | j'_\nu \rangle + \\ & \langle j_\nu | U_k | m' \rangle \langle m | U_k^\dagger | j'_\nu \rangle, \\ e_{j_\nu}^{(k)}(m, m') + i f_{j_\nu}^{(k)}(m, m') = & i \langle j_\nu | U_k | m \rangle \langle m' | U_k^\dagger | j'_\nu \rangle - \\ & i \langle j_\nu | U_k | m' \rangle \langle m | U_k^\dagger | j'_\nu \rangle \end{aligned} \quad (4)$$

[11]. After K experiments, we can setup the matrix equa-

tion

$$M \begin{bmatrix} \rho_{0,0} \\ \vdots \\ \rho_{N-2,N-2} \\ \hline R_{0,1} \\ \vdots \\ R_{0,N-1} \\ \vdots \\ R_{m,m'>m} \\ \vdots \\ R_{N-2,N-1} \\ \hline S_{0,1} \\ \vdots \\ S_{0,N-1} \\ \vdots \\ S_{m,m'>m} \\ \vdots \\ S_{N-2,N-1} \end{bmatrix} = \begin{bmatrix} R_{10,1'_0}^{(1)} \\ \vdots \\ R_{1_\gamma,1'_\gamma}^{(1)} \\ R_{20,2'_0}^{(1)} \\ \vdots \\ R_{n_\gamma,n'_\gamma}^{(K)} \\ \hline S_{10,1'_0}^{(1)} \\ \vdots \\ S_{1_\gamma,1'_\gamma}^{(1)} \\ S_{20,2'_0}^{(1)} \\ \vdots \\ S_{n_\gamma,n'_\gamma}^{(K)} \end{bmatrix}. \quad (5)$$

Here the left column vector is formed by the $N^2 - 1$ unknowns of ρ : diagonal elements in the top, real off-diagonals in the middle, and imaginary off-diagonals in the bottom. The right column vector is formed by KnN numbers - the real and imaginary parts of the experimentally obtained spectral intensities ordered according to the value of the binary string ν , the qubit number j , and the experiment number k . The $KnN \times (N^2 - 1)$ dimensional constraint matrix is of the form

$$M = \begin{bmatrix} a_{1,0}^{(1)}(0,0) & \cdots & c_{1,0}^{(1)}(m,m') & \cdots & e_{1,0}^{(1)}(m,m') & \cdots \\ \vdots & \vdots & \vdots & \vdots & \vdots & \vdots \\ a_{1,\gamma}^{(1)}(0,0) & \cdots & c_{1,\gamma}^{(1)}(m,m') & \cdots & e_{1,\gamma}^{(1)}(m,m') & \cdots \\ \vdots & \vdots & \vdots & \vdots & \vdots & \vdots \\ a_{n,0}^{(1)}(0,0) & \cdots & c_{n,0}^{(1)}(m,m') & \cdots & e_{n,0}^{(1)}(m,m') & \cdots \\ \vdots & \vdots & \vdots & \vdots & \vdots & \vdots \\ \vdots & \vdots & \vdots & \vdots & \vdots & \vdots \\ a_{n,\gamma}^{(K)}(0,0) & \cdots & c_{n,\gamma}^{(K)}(m,m') & \cdots & e_{n,\gamma}^{(K)}(m,m') & \cdots \\ \hline b_{1,0}^{(1)}(0,0) & \cdots & d_{1,0}^{(1)}(m,m') & \cdots & f_{1,0}^{(1)}(m,m') & \cdots \\ \vdots & \vdots & \vdots & \vdots & \vdots & \vdots \\ b_{1,\gamma}^{(1)}(0,0) & \cdots & d_{1,\gamma}^{(1)}(m,m') & \cdots & f_{1,\gamma}^{(1)}(m,m') & \cdots \\ \vdots & \vdots & \vdots & \vdots & \vdots & \vdots \\ b_{n,0}^{(1)}(0,0) & \cdots & d_{n,0}^{(1)}(m,m') & \cdots & f_{n,0}^{(1)}(m,m') & \cdots \\ \vdots & \vdots & \vdots & \vdots & \vdots & \vdots \\ \vdots & \vdots & \vdots & \vdots & \vdots & \vdots \\ b_{n,\gamma}^{(K)}(0,0) & \cdots & d_{n,\gamma}^{(K)}(m,m') & \cdots & f_{n,\gamma}^{(K)}(m,m') & \cdots \end{bmatrix}. \quad (6)$$

Note that each column of the constraint matrix corresponds to contribution of a particular unknown element of ρ to the various spectral intensities.

By choosing the unitaries $\{U_k\}$ such that $\text{rank}(M) \geq$

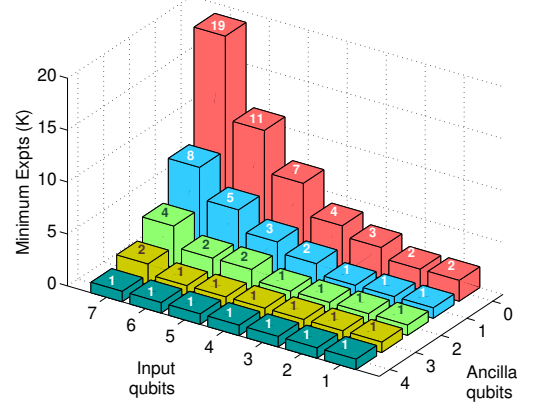


FIG. 1. Minimum number of independent experiments required for QST (with zero ancilla) and AAQST.

$N^2 - 1$ (the number of unknowns), eqn. (5) can be solved either by singular value decomposition or by Gaussian elimination method [11]. Fig. 1 illustrates the minimum number (K) of experiments required for QST. As anticipated, K increases rapidly as $O(N/n)$ with the number of input qubits. In the following we describe how it is possible to speed-up QST, in the presence of an ancilla register, with fewer experiments.

B. Ancilla Assisted QST (AAQST)

Suppose the input register of n -qubits is associated with an ancilla register consisting of \hat{n} qubits. The dimension of the combined system of $\tilde{n} = n + \hat{n}$ qubits is $\tilde{N} = N\hat{N}$, where $\hat{N} = 2^{\hat{n}}$. For simplicity we assume that each qubit interacts sufficiently with all other qubits so as to obtain a completely resolved spectrum yielding $\tilde{n}\tilde{N}$ real parameters. Following method is applicable even if there are spectral overlaps, albeit with lower efficiency (i.e., with higher number (K) of minimum experiments). Further for simplicity, we assume that the ancilla register begins with the maximally mixed initial state, with no contribution to the spectral lines from it. Otherwise, we need to add the contribution of the ancilla to the final spectrum and the eqn. (5) will become inhomogeneous. As explained later in the experimental section, initialization of maximally mixed state can be achieved with high precision. Thus the deviation density matrix of the combined system is $\tilde{\rho} = \rho \otimes \mathbb{1}/\hat{N}$. Now applying only local unitaries neither leads to ancilla coherences nor transfers any of the input coherences to ancilla. Therefore we consider applying a non-local unitary exploiting the input-ancilla interaction,

$$\tilde{U}_k = V \sum_{a=0}^{\hat{N}-1} U_{ka} \otimes |a\rangle\langle a|, \quad (7)$$

where U_{ka} is the k th unitary on the input register dependent on the ancilla state $|a\rangle$ and V is the local unitary on the ancilla. The combined state evolves to

$$\begin{aligned}\tilde{\rho}^{(k)} &= \tilde{U}_k \tilde{\rho} \tilde{U}_k^\dagger \\ &= \frac{1}{\tilde{N}} \sum_{m,m',a} \rho_{mm'} U_{ka} |m\rangle \langle m'| U_{ka}^\dagger \otimes V |a\rangle \langle a| V^\dagger.\end{aligned}\quad (8)$$

We now record the spectrum of the combined system corresponding to the observable $\sum_{j=1}^{\tilde{n}} \sigma_{jx} + i\sigma_{jy}$. Each spectral line can again be expressed in terms of the unknown elements of the ancilla matrix in the form given in eqn. (3). The spectrum of the combined system yields $\tilde{n}\tilde{N}$ linear equations. The minimum number of independent experiments needed is now $O(N^2/(\tilde{n}\tilde{N}))$. Since we can choose $\tilde{N} \gg N$, AAQST needs fewer than $O(N/n)$ experiments required in the standard QST. In particular, when $\tilde{n}\tilde{N} \geq N^2$, a single optimized unitary suffices for QST. Fig. 1 illustrates the minimum number (K) of experiments required for various sizes of input and ancilla registers. As illustrated, QST can be achieved with only one experiment, if an ancilla of sufficient size is provided along with.

C. Building the constraint matrix

The major numerical procedure in AAQST is obtaining the constraint matrix M . For calculating the constraint coefficients $c_{rj}^{(k)}$, one may utilize an elaborate decomposition of U_k using numerical or analytical methods. Alternatively, as described below, we can use a simple algorithmic approach to construct the constraint matrix.

First imagine a diagonal state ρ for the ancilla register (eqn. (2)) with $\rho_{00} = 1$ and $\rho_{mm} = 0$ for all other $1 \leq m \leq N-2$, $R_{mm'} = S_{mm'} = 0$. Applying the unitary U_k on the composite deviation density matrix $\tilde{\rho} = \rho \otimes \mathbb{1}/\tilde{N}$, we obtain all the spectral intensities (using eqn. (3))

$$a_{j\nu}^k(0,0) = R_{j\nu,j\nu}^{(k)}, \quad b_{j\nu}^k(0,0) = S_{j\nu,j\nu}^{(k)}.\quad (9)$$

Thus the spectral lines indicate the contributions only from ρ_{00} (and $\rho_{N-1,N-1}$). Repeating the process with all the unitaries $\{U_k\}$ yields the first column in M matrix (eqn. (6)) corresponding to the unknown ρ_{00} . Same procedure can be used for all the diagonal elements ρ_{mm} with $0 \leq m \leq N-2$.

To determine M matrix column corresponding to a real off-diagonal unknown $R_{mm'}$, we start with an input-register density matrix $R_{mm'} = 1$ and all other elements set to zero. Again by applying the unitary U_k on the composite density matrix, and using eqn. (3) we obtain

$$c_{j\nu}^k(m,m') = R_{j\nu,j\nu}^{(k)}, \quad d_{j\nu}^k(m,m') = S_{j\nu,j\nu}^{(k)}.\quad (10)$$

Repeating the process with all unitaries $\{U_k\}$ determines the column of M corresponding to the unknown $R_{mm'}$.

To determine M matrix column corresponding to an imaginary off-diagonal unknown $S_{mm'}$, we set $S_{mm'} = 1$ and all other elements to zero, and apply U_k on the composite state to obtain

$$e_{j\nu}^k(m,m') = R_{j\nu,j\nu}^{(k)}, \quad f_{j\nu}^k(m,m') = S_{j\nu,j\nu}^{(k)}.\quad (11)$$

Proceeding this way, by selectively setting the unknowns one by one, the complete constraint matrix can be built easily.

D. Optimization of Unitaries

Solving the matrix equation (5) requires that $\text{rank}(M) \geq N^2 - 1$, the number of unknowns. But having the correct rank is not sufficient. The matrix M must be well conditioned in order to ensure that small errors in the observed intensities $\{R_{j\nu,j\nu}^{(k)}, S_{j\nu,j\nu}^{(k)}\}$ do not contribute to large errors in the values of the elements $\rho_{mm'}$. The quality of the constraint matrix can be measured by a scalar quantity called condition number $C(M)$ defined as the ratio of the largest singular value of M to the smallest [12]. Smaller the value of $C(M)$, better conditioned is the constraint matrix M for solving the unknowns. Thus the condition number provides a convenient scalar quantity to optimize the set $\{U_k\}$ of unitaries to be selected for QST. As explained in the experimental section, we used a simple unitary model $U_1(\tau_1, \tau_2)$ as an initial guess and used genetic algorithm to minimize the condition number and optimize the parameters (τ_1, τ_2) .

The necessary number (K) of independent experiments is decided by the rank of the constraint matrix and the desired precision. The rank condition requires that $K n N \geq N^2 - 1$. Introducing additional experiments renders the problem over-determined, thus reducing the condition number and increasing the precision. In the following section we describe the experimental results of AAQST for registers with (i) $n = 2, \hat{n} = 1, \tilde{n} = 3$ and (ii) $n = 3, \hat{n} = 2, \tilde{n} = 5$ respectively.

III. EXPERIMENTS

We report experimental demonstrations of AAQST on two spin-systems of different sizes and environments. In each case, we have chosen two density matrices for tomography. All the experiments described below are carried out on a Bruker 500 MHz spectrometer at an ambient temperature of 300 K using high-resolution nuclear magnetic resonance techniques.

A. Two-qubit input, One-qubit ancilla

Here we use three spin-1/2 ^{19}F nuclei of iodotrifluoroethylene ($\text{C}_2\text{F}_3\text{I}$) dissolved in acetone- D_6 as a 3-qubit

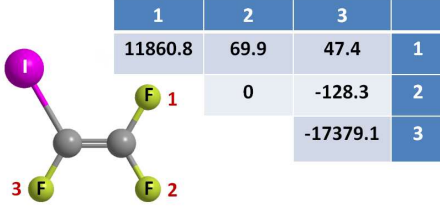


FIG. 2. Molecular structure of iodotrifluoroethylene, and the table of Hamiltonian parameters in Hz: chemical shifts (diagonal elements) and J-coupling constants (off-diagonal elements).

system. The molecular structure and the Hamiltonian parameters are shown in Fig. 2. As can be seen in Fig. 3, all the 12 transitions of this system are clearly resolved.

We have chosen F_1 as the ancilla qubit and F_2 and F_3 as the input qubits. QST was performed for two different density matrices (i) thermal equilibrium state, i.e., $\rho_1 = \frac{1}{2}(\sigma_z^2 + \sigma_z^3)$, and (ii) state after a $(\pi/4)_{\pi/4}$ pulse applied to the thermal equilibrium state, i.e., $\rho_2 = \frac{1}{2}(\sigma_x^2 + \sigma_x^3) - \frac{1}{2}(\sigma_y^2 + \sigma_y^3) + \frac{1}{\sqrt{2}}(\sigma_z^2 + \sigma_z^3)$. In both the cases, the first qubit was initialized into a maximally mixed state by applying a selective $(\pi/2)_y$ pulse on F_1 and followed by a strong pulsed-field-gradient (PFG) in the z -direction. The selective pulse was realized by GRAPE technique [13].

AAQST of each of the above density matrices required just one unitary evolution followed by the measurement of complex NMR signal. We modelled the AAQST unitary as follows: $U_1 = (\frac{\pi}{2})_y U_{\text{int}}(\tau_2) (\frac{\pi}{2})_x U_{\text{int}}(\tau_1)$, where $U_{\text{int}}(\tau) = \exp(-i\mathcal{H}\tau)$ is the unitary operator for evolution under the internal Hamiltonian \mathcal{H} (see eqn. (1)) for a time τ , and $(\frac{\pi}{2})$ rotations are realized by non selective radio frequency pulses applied to all the spins along the directions indicated by the subscripts. The constraint matrix M had 15 columns corresponding to the unknowns and 24 rows corresponding to the real and imaginary parts of the 12 spectral lines. Only the durations $\{\tau_1, \tau_2\}$ needed to be optimized to minimize the condition number $C(M)$. We used a genetic algorithm for the optimization and obtained $C(M) = 17.3$ for $\tau_1 = 6.7783$ ms and $\tau_2 = 8.0182$ ms. The real and imaginary parts of the single shot experimental AAQST spectrum, along with the reference spectrum, are shown in the top part of Fig. 3. The intensities $\{R_{j\nu, j\nu'}^{(1)}, S_{j\nu, j\nu'}^{(1)}\}$ were obtained by simple curve-fit routines, and the matrix eqn. (5) was solved to obtain all the unknowns. The reconstructed density matrices along with the theoretically expected ones are shown below the spectra in Fig. 3. The fidelities of experimental states with the theoretically expected states (ρ_1 and ρ_2) are respectively 0.998 and 0.990. The high fidelities indicated successful AAQST of the prepared states.

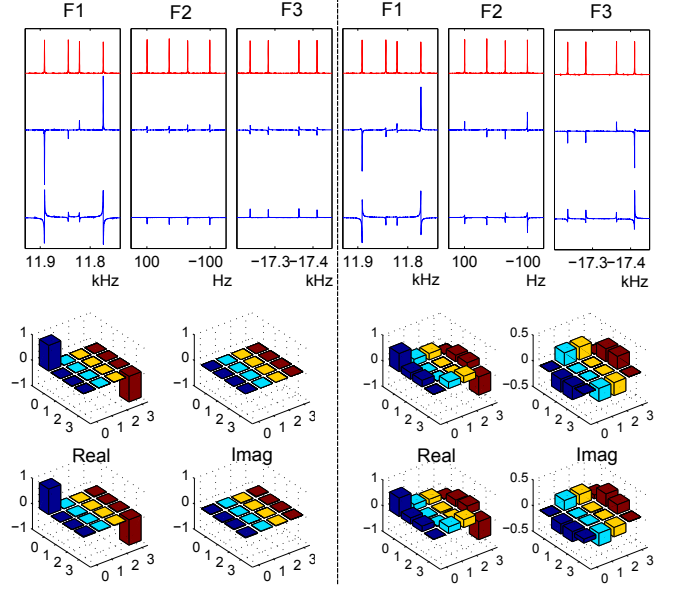


FIG. 3. AAQST results for thermal equilibrium state ρ_1 (left column), and that of state ρ_2 (right column), described in the text. The reference spectra is in the top trace. The spectra corresponding to the real part ($R_{j\nu, j\nu'}^{(1)}$, middle trace) and the imaginary part ($S_{j\nu, j\nu'}^{(1)}$, bottom trace) of the ^{19}F signal are obtained in a single shot AAQST experiment. The bar plots correspond to theoretically expected states (top row) and those obtained from AAQST experiments (bottom row). Fidelities of the states are 0.997 and 0.99 respectively for the two density matrices.

B. Three-qubit input, Two-qubit ancilla

We use three ^{19}F nuclei and two ^1H nuclei of 1-bromo-2,4,5-trifluorobenzene partially oriented in a liquid crystal namely, N-(4-methoxybenzaldehyde)-4-butylaniline (MBBA). Due to the partial orientational order, the direct spin-spin interaction (dipolar interaction) does not get fully averaged out, but gets scaled down by the order parameter [14]. The chemical shifts and the strengths of

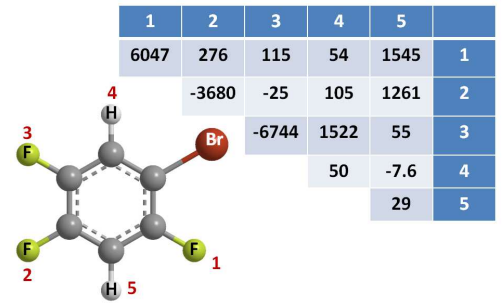


FIG. 4. Molecular structure of 1-bromo-2,4,5-trifluorobenzene, and the table of Hamiltonian parameters in Hz: chemical shifts (diagonal elements) and effective coupling constants ($J+2D$)(off-diagonal elements).

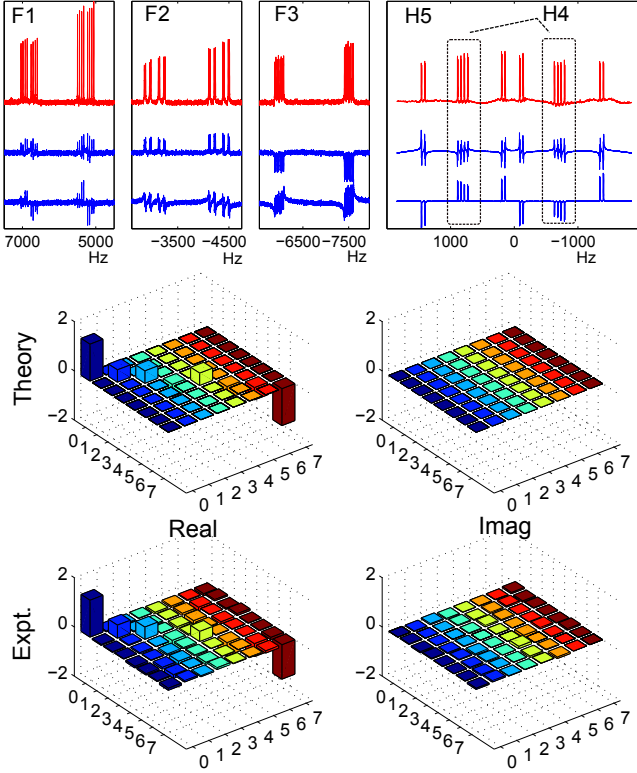


FIG. 5. AAQST results for thermal equilibrium state, i.e., $(\sigma_z^1 + \sigma_z^2 + \sigma_z^3)/2$. The reference spectrum is in the top trace. The spectra corresponding to the real part ($R_{j\nu,j\nu'}^{(1)}$, middle trace) and the imaginary part ($S_{j\nu,j\nu'}^{(1)}$, bottom trace) of the ^{19}F signal are obtained in a single shot AAQST experiment. The bar plots correspond to theoretically expected states (top row) and those obtained from AAQST experiments (bottom row). Fidelity of the AAQST state is 0.98.

the effective couplings are shown in Fig. 4. As is evident, the partially oriented system can display stronger and longer-range coupling network leading to a larger register. Here we choose the three ^{19}F nuclei forming the input register and two ^1H nuclei forming the ancilla register. The Hamiltonian for the heteronuclear dipolar interaction (between ^1H and ^{19}F) has an identical form as that of J-interaction [14]. The homonuclear dipolar couplings (among ^{19}F , as well as among ^1H nuclei) were small compared to their chemical shift differences enabling us to approximate the Hamiltonian in the form of eqn. (1).

The partially oriented spin-system yields all the 80 transitions sufficiently resolved. Again we use just one experiment for the complete AAQST of the 3-qubit input register. We modelled the AAQST unitary in a similar way as before: $U_1 = (\frac{\pi}{2})_x U_{\text{int}}(\tau_2) (\frac{\pi}{2})_x U_{\text{int}}(\tau_1)$ where

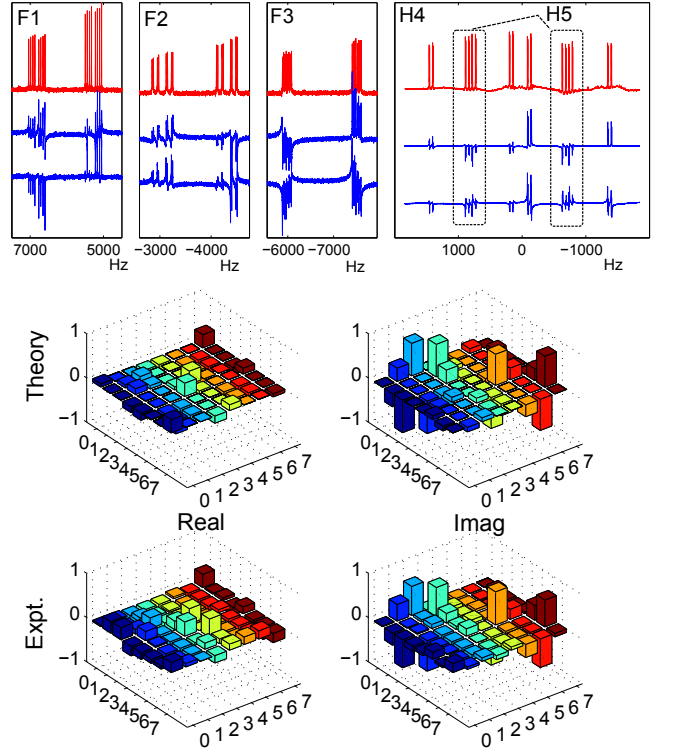


FIG. 6. AAQST results for the state ρ_2 described in the text. The reference spectrum is in the top trace. The real (middle trace) and the imaginary spectra (bottom trace) are obtained in a single shot AAQST experiment. The bar plots correspond to theoretically expected states (top row) and those obtained from AAQST experiments (bottom row). Fidelity of the AAQST state is 0.95.

$U_{\text{int}}(\tau) = \exp(-i\mathcal{H}\tau)$ is the unitary operator for evolution under the internal Hamiltonian \mathcal{H} (see eqn. (1)) for a time τ , and $(\frac{\pi}{2})_x$ are global x-rotations. The constraint matrix M had 63 columns corresponding to the unknowns and 160 rows corresponding to the real and imaginary parts of 80 spectral lines. After optimizing the durations by minimizing the condition number using a genetic algorithm, we obtained $C(M) = 14.6$ for $\tau_1 = 431.2 \mu\text{s}$ and $\tau_2 = 511.5 \mu\text{s}$. Again we study AAQST on two states: (i) Thermal equilibrium of the ^{19}F spins: $\rho_1 = (\sigma_z^1 + \sigma_z^2 + \sigma_z^3)/2$, and (ii) a random density matrix ρ_2 obtained by applying unitary $U_0 = (\frac{\pi}{2})_x^F \tau_0 (\pi)_x^H \tau_0 (\frac{\pi}{2})_y^{F_1}$, with $\tau_0 = 2.5 \text{ ms}$, on thermal equilibrium state, i.e., $\rho_2 = U_0 \rho_1 U_0^\dagger$. In both the cases, we initialize the ancilla i.e., the ^1H qubits on to a maximally mixed state by first applying a $(\pi/2)^H$ pulse followed by a strong PFG in the z -direction.

The real and imaginary parts of the single shot AAQST spectra, along with the reference spectra, are shown in Figs. 5 and 6 respectively. Again the line intensities $\{R_{j\nu,j\nu'}^{(1)}, S_{j\nu,j\nu'}^{(1)}\}$ are obtained by curve-fitting, and all the 63 unknowns of the 3-qubit deviation density matrix are obtained by solving the matrix eqn. (5). The

reconstructed density matrices along with the theoretically expected states (ρ_1 and ρ_2) are shown below the spectra in Figs. 5 and 6. The fidelities of experimental states with the theoretically expected states (ρ_1 and ρ_2) are respectively 0.98 and 0.95. The lower fidelity in the latter case is mainly due to the imperfections in the preparation of the target state ρ_2 . The overall poorer performance in the liquid crystal system is due to the lower fidelities of the QST pulses, spatial and temporal variations of solute order-parameter, and stronger decoherence rates compared to the isotropic case. In spite of these difficulties, the three-qubit density matrix with 63 unknowns could be estimated quantitatively through a single NMR experiment.

IV. CONCLUSIONS

Quantum state tomography is an important part of experimental studies in quantum information processing. The standard method involves a large number of independent measurements to reconstruct a density matrix. The ancilla-assisted quantum state tomography introduced by Nieuwenhuizen and co-workers allows complete reconstruction of complex density matrix with fewer experiments by letting the unknown state of the input register to interact with an ancilla register initialized in a known state. Ancilla registers are essential in many of the quantum algorithms. Usually, at the end of the

quantum algorithms, ancilla is brought to a state which is separable with the input register. The same ancilla register which is used for computation can be utilized for tomography after the computation. The ancilla register can be prepared into a maximally mixed state by dephasing all the coherences and equalizing the populations.

We provided methods for explicit construction of tomography matrices in large registers. We also discussed the optimization of tomography experiments based on minimization of the condition number of the constraint matrix. Finally, we demonstrated the experimental ancilla-assisted quantum state tomography in two systems: (i) a system with two input qubits and one ancilla qubit in an isotropic medium and (ii) a system with three input qubits and two ancilla qubits in a partially oriented medium. In both the cases, we successfully reconstructed the target density matrices with a single quadrature detection of transverse magnetization. The methods introduced in this work should be useful for extending the range of quantum state tomography to larger registers.

ACKNOWLEDGEMENTS

The authors are grateful to Mr. Hemant Katiyar, Dr. Soumya S. Roy, and Prof. Anil Kumar for discussions. This work was partly supported by DST project SR/S2/LOP-0017/2009.

-
- [1] M. A. Nielsen and I. L. Chuang, *Quantum Computation and Quantum Information* (Cambridge University Press, 1994).
 - [2] H. O. Everitt, ed., *Experimental Aspects of Quantum Computing* (Springer US, 2005).
 - [3] I. L. Chuang, N. Gershenfeld, M. G. Kubinec, and D. W. Leung, Proc. Roy. Soc. Lond. A **454**, 447 (1998).
 - [4] D. Leung, L. Vandersypen, X. Zhou, M. Sherwood, C. Yannoni, M. Kubinec, and I. L. Chuang, Phys. Rev. A **60**, 1924 (1999).
 - [5] R. Das, T. S. Mahesh, and A. Kumar, Phys. Rev. A **67**, 062304 (2003).
 - [6] A. E. Allahverdyan, R. Balian, and T. M. Nieuwenhuizen, Phys. Rev. Lett. **92**, 120402 (2004).
 - [7] X. Peng, J. Du, and D. Suter, Phys. Rev. A **76**, 042117 (2007).
 - [8] Y. Yu, H. Wen, H. Li, and X. Peng, Phys. Rev. A **83**, 032318 (2011).
 - [9] J. Cavanagh, W. J. Fairbrother, A. G. Palmer, and N. J. Skelton, *Protein NMR spectroscopy: principles and practice* (Academic Pr, 1996).
 - [10] D. G. Cory, A. F. Fahmy, and T. F. Havel, Proc. Natl. Acad. Sci. USA **94**, 1634 (1997).
 - [11] S. S. Roy and T. S. Mahesh, J. Magn. Reson. **206**, 127 (2010).
 - [12] L. N. Trefethen and D. A. Bau, *Numerical Linear Algebra* (SIAM, 1997).
 - [13] N. Khaneja, T. Reiss, C. Kehlet, T. Schulte-Herbruggen, and S. J. Glaser, *J. Magn. Reson.* **172**, 296 (2005).
 - [14] R. Y. Dong, *Nuclear Magnetic Resonance of Liquid Crystals* (Springer, 1997).